IEEE Access
Multidisciplinary | Rapid Review | Open Access Journal

Received 5 February 2023, accepted 26 February 2023, date of publication 6 March 2023, date of current version 22 March 2023.

Digital Object Identifier 10.1109/ACCESS.2023.3253205

METHODS

Implementation of Digital Beamforming System for Microwave Power Transfer With Real-Time Beam Scanning

MINJAE AHN[1], (Student Member, IEEE), INHO PARK[2], (Member, IEEE), ILLSOO SOHN[3], (Member, IEEE), OH-SOON SHIN[4], (Member, IEEE), AND HYUNCHUL KU[1], (Member, IEEE)

[1]Department of Electronics, Information and Communication Engineering, Konkuk University, Seoul 05029, South Korea
[2]Hanwha Systems Company Ltd., Yongin-si 17121, South Korea
[3]Department of Computer Science and Engineering, Seoul National University of Science and Technology, Seoul 01811, South Korea
[4]Department of Electronic Engineering, Soongsil University, Seoul 06978, South Korea

Corresponding author: Hyunchul Ku (hcku@konkuk.ac.kr)

This work was supported in part by the National Research Foundation of Korea (NRF) Grant (NRF-2017R1A5A1015596) funded by the Korean Government (MSIT), and in part by the NRF Grant (NRF-2020R1F1A1061826) funded by the Korean Government (MSIP).

ABSTRACT In this study, we propose a digital beamforming system for microwave power transfer with a real-time beam-scanning algorithm for tracking a moving receiver. To perform scanning, each channel in the transmitter generates and converts a baseband signal for the allocated beam direction based on the pilot slots in a frame structure. An initial timer reset process and a preamble are included in the algorithm to maintain time synchronization among units of the scanning period in a wireless environment. The average received power is simulated, and the optimal frame configuration is derived by considering the proportion of an energy transmission slot in the frame. For experimental verification, we design a 4×4 digital beamforming system operating at 5.8 GHz and a receiver. The scanning performance is experimentally validated with various numbers of scanning beams and placements of the receiver. Moreover, when radiating 16 W of RF power, an RF power of 100 mW or more is received in all sections for the scenario of the receiver moving in a 1 m distance using 1 second period beam scanning. The proposed microwave power transfer system with a real-time beam scanning algorithm is verified to track the moving receiver in a wireless environment and perform optimal microwave power transfer.

INDEX TERMS Beam scanning, digital beamforming, frame structure, microwave power transfer.

I. INTRODUCTION

With the development of information and communication technology, there is an increasing interest in wireless power transfer (WPT) for IoT devices. Among the numerous WPT technologies, microwave power transfer (MPT) using beamforming can wirelessly transmit power to a receiver (Rx) over a long distance; therefore, many studies are being conducted [1], [2]. System implementation and application for MPT have been developed mainly based on industrial, scientific, and medical (ISM) bands [3]. In MPT, the power transfer efficiency is lowered if beamforming cannot be accurately performed at the position of the Rx [4]. In addition, in the case of a moving Rx, the tracking period is crucial because the position continuously changes.

Studies on Rx tracking methods based on the received power have been underway [5], [6], [7], [8], [9], [10], [11], [12]. Generally, these studies have used a frame structure that divides time into frames with several pilot slots and one energy transmission slot. The optimal phase set of the transmitter (Tx) for achieving the maximum received power is specified based on the received power while radiating the pilot slots. In [5], the ordinary least squares method and Kalman filter-based algorithm were proposed, and it was

The associate editor coordinating the review of this manuscript and approving it for publication was Alon Kuperman.

verified that the optimal phase set could be obtained via simulations. In [6], a 64-channel analog beamforming system was designed to verify an algorithm previously studied in [5]. Accordingly, 13.7 mW of RF power was received when 9.5 W of power was radiated from the transmit antenna at 25 m. Additionally, there are look-up table (LUT)-based MPT studies where pilot slots are radiated based on predefined phase sets and an optimal phase set that receives the maximum received power is selected. The authors of [7] proposed a focal beamforming algorithm for application in far-field and near-field regions, and they designed a 32-channel analog beamforming system. Moreover, they confirmed that 191.1 mW of DC power was received when 16 W of power was radiated from the transmitting antenna at 1 m. In [8], a beam-scanning algorithm capable of covering far-field and near-field regions was proposed. Moreover, a 64-channel analog beamforming system was developed, and it was verified that 12.4 mW of DC power was received when 10.33 W of power was radiated from the Tx array at 10 m. The aforementioned studies found the optimal phase set by radiating the pilot slot based on the defined phase sets; however, there was no validity for the number of pilot slots. In a scenario where the position of the Rx needs to be repeatedly updated, its analysis is needed since the time proportion of the energy transmission slot in the frame is related to the average received power. Moreover, there have been no reports of experimentally verified studies in a wireless environment, and the system was only verified by connecting the Rx using a wire. Therefore, the performance should be analyzed based on the number of pilot slots, and a system that can operate in a fully wireless environment is required for WPT. As Rx operates on the received energy, its architecture should have low power consumption when processing information (i.e., decoding and feedback) [13]. Studies have verified the beamforming algorithms by considering Rx in a wireless environment [9], [10], [11], [12]. The authors of [9] used the time reversal method using a pilot signal from Rx for tracking; it takes 0.8 s to track and perform MPT. In [10], the channels were estimated using received signal strength indicator(RSSI) feedback. An optimal value for each channel is obtained; however, the measurement and feedback interval per RSSI was set to 0.5 s considering the power consumption of Rx. Generally, [9] and [10] are effective when the channel changes at a slower rate; however, a shorter tracking time is required to perform MPT for a moving receiver in real time. References [11] and [12] used digital beamforming (DBF) for validating a MPT algorithm based on baseband signal samples. The authors of [11] designed a system to update the beamforming weight of Tx by feeding back RSSI iteratively. In [12], the period of a frame for channel estimation is 100 ms, which shows that DBF can effectively configure short slots in the frame structure. It converges to the optimal beam through several frames. In the experiment, the Rx tracking speed exhibits a large deviation (up to 14 s) for each moving case.

In this study, we designed a digital beamforming system for MPT with real-time tracking. The proposed beam-scanning algorithm employs a frame structure that includes several pilot slots and one energy transmission slot. In the pilot slot, beamforming was performed based on the phase sets calculated using the far-field approximation in the antenna theory. The time per scanning can be reduced because slots are set at the baseband signal using DBF. Among the phase sets, the one with the maximum received power was selected as the optimal beam direction for the MPT. Beamforming for energy transfer was then performed in the energy transmission slot by applying the optimal direction. Optimal power transfer can be performed for each frame period because the algorithm has low complexity with predefined phase sets. The received power was analyzed based on the proposed algorithm, and the number of pilot slots required for maximum efficiency was presented. For verification, a 16-channel DBF system was designed at 5.8 GH; it has an advantage in implementing a compact system with a band higher than other ISM bands, 915 MHz, and 2.4 GHz. Moreover, we designed an Rx equipped with a communication module (CMM) to transmit an index of maximum received power to the Tx. In information decoding, a simple receiver architecture was adopted for rectifying the signal in each scanning slot and sampling it as a single voltage value via ADC. In addition, an initial timer reset process and a preamble in the frame were included for time synchronization in a wireless environment. We experimentally verify the beam scanning of the system for various placements of Rx and numbers of scanning beams. Additionally, we confirm that MPT can be performed while tracking Rx in real time via the Rx tracking experiment with a scanning time of 0.126 s. Compared to other existing LUT-based works, the implemented system can test algorithms in a fully wireless environment. Furthermore, with DBF, this work can rapidly switch the phase of each channel for scanning and energy transmission while maintaining time synchronization.

The remainder of this paper is organized as follows. In Section II, the beam scanning algorithm is described. Section III presents the design and implementation of the MPT system. In Section IV, the experimental procedure and results are presented, and the system performance is discussed. Finally, Section V presents the conclusions of this study.

II. BEAM SCANNING ALGORITHM

A schematic of the proposed beam-scanning algorithm is depicted in Fig. 1. To trackRx, the received power is checked via beam scanning, which changes the direction of the beam radiated from the $M \times N$ planar array antenna L times. The steering direction for the Rx is determined based on the largest

power among the received powers, and the energy is transmitted to the corresponding position. Figure 2 illustrates the frame structure used in the proposed algorithm. The frame

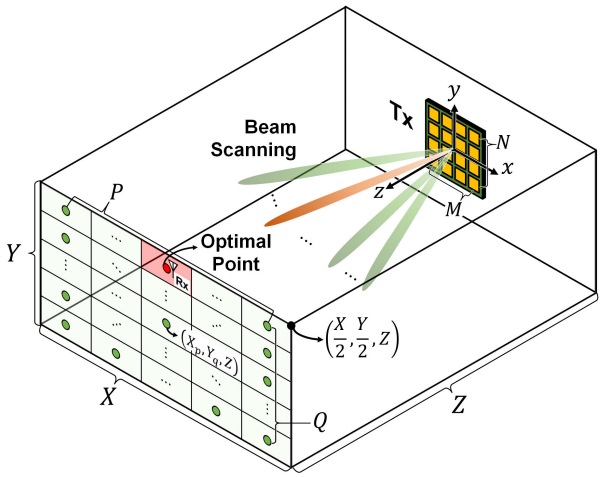

FIGURE 1. Schematic of the beam scanning algorithm.

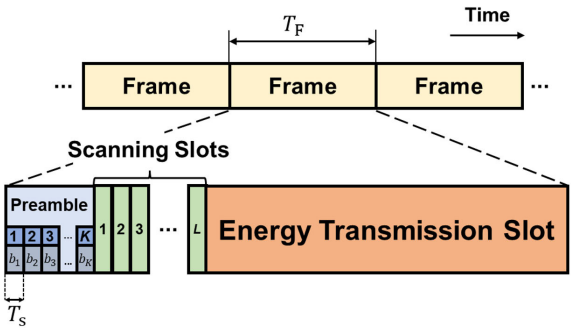

FIGURE 2. Frame structure of the beam scanning algorithm.

structure comprises K pilot slots as the preamble, L pilot slots for beam scanning, and an energy transmission slot. The entire frame time is denoted as T_{F} and the pilot interval is T_{s}. In this section, the beam-scanning algorithm is mathematically expressed based on the baseband signal generated from each channel of the array antenna and the received power.

The preamble is the pilot signal used to determine the start of the scanning slot index. On-off keying modulation was selected as the modulation for the preamble, where b_k denotes the bit signal of the k-th preamble slot. As depicted in Fig. 1, X, Y, and Z indicate the sizes of the space for the definition of direction in the beam scanning following the preamble. The center of the Tx array antenna is assumed to be the origin, and Z indicates the distance set as a reference for the calculation of the direction. Moreover, P and Q represent the number of points for beamforming on the x-axis and y-axis, respectively, and the position for the (p, q) point is expressed as follows

$$X_p = -\frac{X}{2} + \frac{X}{2P}(2p-1) \quad (p = 1, 2, \cdots, P), \tag{1}$$

$$Y_q = \frac{Y}{2} - \frac{Y}{2Q}(2q-1) \quad (q = 1, 2, \cdots, Q). \tag{2}$$

Equations (1) and (2) define the x- and y-positions of the (p, q) point, respectively, which is in the p-th index along the x-axis and the q-th index along the y-axis expressed in the Cartesian coordinate system. The direction of the (p, q) point system in the spherical coordinate system is expressed as

$$\theta_{p,q} = \cos^{-1}\left(\frac{Z}{\sqrt{X_p^2 + Y_q^2 + Z^2}}\right), \tag{3}$$

$$\phi_{p,q} = \tan^{-1}\left(\frac{Y_q}{X_p}\right). \tag{4}$$

Equations (3) and (4) describe the azimuth angle ($\phi_{p,q}$) and elevation angle ($\theta_{p,q}$) of point (p, q), respectively. Because the proposed algorithm sequentially radiates the beams $L(=PQ)$ times, the direction of the L beams can be expressed as a $1 \times L$ vector, as follows:

$$\boldsymbol{u}_q = \left[\theta_{1,q}\ \theta_{2,q}\ \cdots\ \theta_{P,q}\right], \tag{5}$$

$$\boldsymbol{\theta} = \left[\boldsymbol{u}_1\ \boldsymbol{u}_2\ \cdots\ \boldsymbol{u}_Q\right], \tag{6}$$

$$\boldsymbol{v}_q = \left[\phi_{1,q}\ \phi_{2,q}\ \cdots\ \phi_{P,q}\right], \tag{7}$$

$$\boldsymbol{\phi} = \left[\boldsymbol{v}_1\ \boldsymbol{v}_2\ \cdots\ \boldsymbol{v}_Q\right]. \tag{8}$$

As in (6) and (8), it can be expressed as $1 \times L$ vectors; the l-th element of (6) is defined as θ_l, and the l-th element of (8) is defined as ϕ_l. Therefore, based on the far-field approximation in antenna theory [14], a $1 \times L$ vector with a phase required for the (m, n) Tx element in the array antenna for beam steering toward the l-th point as its element can be expressed as follows:

$$\boldsymbol{\psi}_{m,n} = \left[e^{j\psi_{m,n}^{(1)}}\ e^{j\psi_{m,n}^{(2)}}\ \cdots\ e^{j\psi_{m,n}^{(L)}}\right], \tag{9}$$

where

$$\psi_{m,n}^{(l)} = -\beta\left\{(m-1)\,d_x \sin\theta_l \cos\phi_l + (n-1)\,d_y \sin\theta_l \sin\phi_l\right\}, \tag{10}$$

where β symbolizes the wave number, and d_x and d_y represent the spacings between the elements in the x- and y-axis array elements, respectively. To express a complex envelope signal based on (9), a $1 \times L$ vector with a baseband signal as its element is expressed as

$$\boldsymbol{c} = \left[c_1\ c_2\ \cdots\ c_L\right]^T, \tag{11}$$

where

$$c_l = a_{K+l} e^{j2\pi f_b t} \tag{12}$$

$$a_i = \begin{cases} 1, & \{(i-1)\,T_{\mathrm{s}} \le t < iT_{\mathrm{s}}\} \\ 0, & \text{otherwise} \end{cases} \tag{13}$$

where f_b denotes the frequency of the baseband signal. Equation (12) is a continuous-wave (CW) expression that constitutes the baseband signal for the l-th pilot slot. From (13), the CW term, except c_l, is not involved in the l-th beam scanning slot. The baseband signal of the (m, n)

Tx element can be expressed as

$$\tilde{x}_{m,n}(t) = \begin{cases} \sum_{i=1}^{K} U_{m,n} a_i b_i e^{j2\pi f_b t} \\ \qquad (0 \le t < KT_s) \\ \boldsymbol{\psi}_{m,n}\boldsymbol{c} = \sum_{i=1}^{L} a_{K+i} e^{j\left(2\pi f_b t + \psi_{m,n}^{(i)}\right)} \\ \qquad \{KT_s \le t < (K+L)T_s\} \\ e^{j\left(2\pi f_b t + \psi_{m,n}^{(l_{\max})}\right)} \\ \qquad \{(K+L)T_s \le t < T_F\} \end{cases}, \quad (14)$$

where $U_{m,n}$ indicates whether the (m, n) Tx element is used for signal transmission in the preamble slots, and $l_{\max}$ indicates the index of the scanning slot at which the maximum received power is measured. A passband signal obtained by up-converting the frequency (14) can be expressed as follows:

$$x_{m,n}(t) = Re\left\{\tilde{x}_{m,n}(t)\, e^{j2\pi f_c t}\right\}, \quad (15)$$

where f_c denotes the carrier frequency. Each element of the array antenna emits an RF signal, as indicated in (15).

$U_{m,n}$ is set such that the Rx can receive a preamble signal at all (p, q) points. A subset was selected from the entire array antenna, and an array factor (AF) was utilized to determine the subset. The array factor when the $M_{\text{pre}} \times N_{\text{pre}}$ subarray radiates in the (0°,0°) direction is expressed as

$$\text{AF}_{\text{pre}}(\theta, \phi) = \sum_{n=1}^{N_{\text{pre}}} \left[\sum_{m=1}^{M_{\text{pre}}} e^{j\beta(m-1)d_x \sin\theta\cos\phi} \right] e^{j\beta(n-1)d_y \sin\theta\sin\phi}. \quad (16)$$

By calculating $\text{AF}_{\text{pre}}(\boldsymbol{\theta}, \boldsymbol{\phi})$, M_{pre} and N_{pre} were determined as the sizes of the largest possible subarrays satisfying $|\text{AF}_{\text{pre}}| \ge 1$ for all (p, q) points. $|\text{AF}_{\text{pre}}| \ge 1$ indicates that the radiation pattern is higher than that of a single Tx element transmission. For the $M_{\text{pre}} \times N_{\text{pre}}$ subarray, $U_{m,n}$ is defined as follows:

$$U_{m,n} = \begin{cases} 1 \\ \left| m - \frac{M}{2} - \frac{1}{4} \right| \le \frac{M_{\text{pre}}}{2} - \frac{1}{4} \\ \text{and } \left| n - \frac{N}{2} - \frac{1}{4} \right| \le \frac{N_{\text{pre}}}{2} - \frac{1}{4} \\ 0 \\ \quad \text{otherwise} \end{cases}. \quad (17)$$

In Algorithm 1, we summarize the beam scanning algorithm in Tx.

To mathematically express the process of determining $l_{\max}$, we consider the power received by the l-th scanning beam. Based on [15], an equation for the received RF power is derived by the superposition of electric fields radiated from individual Tx elements, which is given as follows:

$$P_R^{(l)} = \left(\frac{\lambda}{4\pi}\right)^2 \left| \sum_{n=1}^{N} \sum_{m=1}^{M} \sqrt{P_{T_{m,n}} G_{T_{m,n}} G_{R_{m,n}}} \frac{e^{-j\left(\beta r_{m,n} + \psi_{m,n}^{(l)}\right)}}{r_{m,n}} \right|^2, \quad (18)$$

where λ denotes the wavelength, $P_{T_{m,n}}$ indicates the excited power to the (m, n) Tx element, $G_{T_{m,n}}$ indicates the realized gain in the direction from the (m, n) Tx element to the Rx, $G_{R_{m,n}}$ corresponds to the realized gain in the direction from the Rx element to the (m, n) Tx element, and $r_{m,n}$ denotes the distance from the (m, n) Tx element to the Rx position. Here, (18) considers that there is one receiving antenna and expresses the power received by the l-th scanning beam. Because the power of the RF signal applied to the Rx antenna is given by (18), the rectified power via an RF-DC converter that rectifies the RF signal into a DC signal can be written as follows:

$$P_{\text{DC}}^{(l)} = \eta_{\text{RF-DC}} P_R^{(l)}, \quad (19)$$

where $\eta_{\text{RF-DC}}$ indicates the efficiency of the RF-DC converter. Moreover, a DC voltage ($V_{\text{DC}}^{(l)}$) of the converter in Rx is applied owing to the rectified DC power. In the proposed algorithm, the index of the maximum voltage is transferred to Tx among the DC voltage values applied to the converter, and the beam direction is reconfigured based on the optimal index. Therefore, using the beam-scanning algorithm, a total of L received DC voltages can be obtained, and an optimal index can be expressed as follows:

$$l_{\max} = \arg\max_{l} \left\{ V_{\text{DC}}^{(l)} \right\}, \quad (20)$$

$$P_{\max} = P_R^{(l_{\max})}. \quad (21)$$

Therefore, in the energy slot of the frame structure, the power is transferred to the $l_{\max}$ point, and the maximum received power is obtained using (21).

Algorithm 1 Beam Scanning Algorithm

1:**Initialize**: Divide the space to be scanned into $P \times Q$ points and allocate x- and y-position $X_p$and Y_q via Eq. (1) – (2);
2:Set the beam direction vectors θ and ϕ via Eq. (3) – (8);
3:Calculate the phase vectors $\psi_{m,n}$ for each antenna element according to Eq. (9) – (10);
4:Determine Tx elements to be used for preamble transmission $U_{m,n}$ via Eq. (16) – (17);
5:**Repeat**: ▷ Eq. (14) – (15)
6: Transmit K bits with On-off keying modulation as the preamble during KT_s;
7: Transmit the L beams sequentially for scanning while changing the beam direction based on θ and ϕ during LT_s;
8: Perform MPT with $l_{\max}$ -th beam during T_F-$(K + L)T_s$;
9: Update $l_{\max}$ from feedback during MPT via Eq. (20);
10:**End**

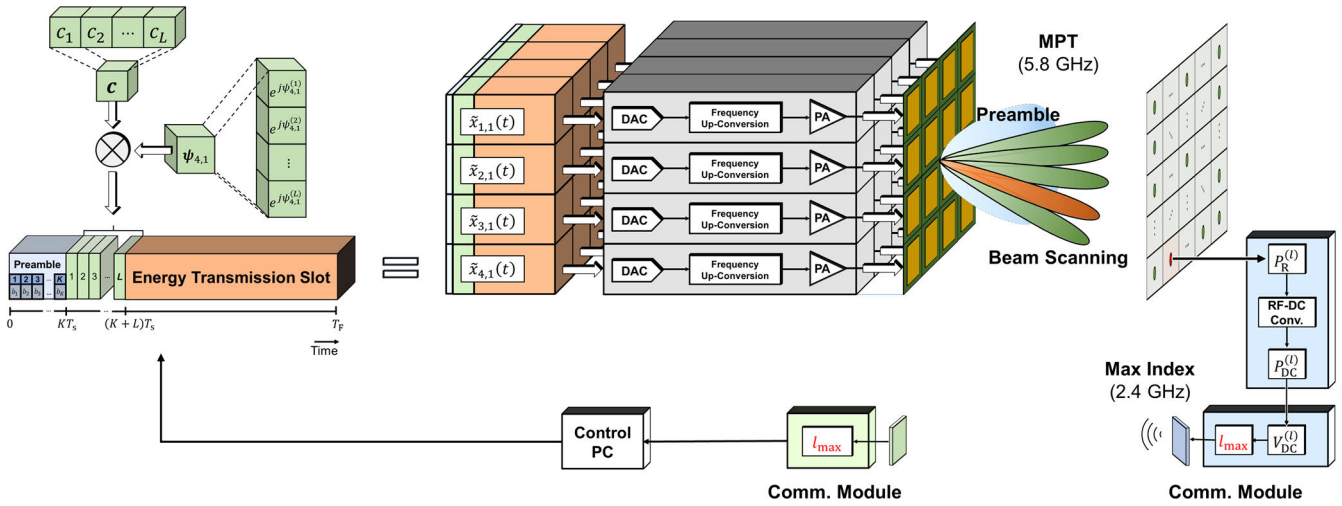

FIGURE 3. Block diagram of the beam-scanning system with the proposed algorithm.

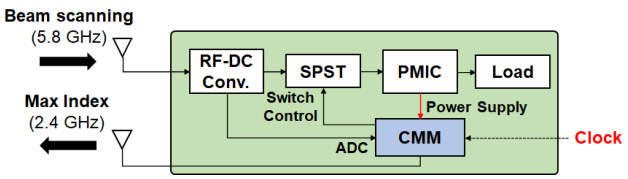

FIGURE 4. Block diagram of Rx.

III. SYSTEM DESIGN

A. SYSTEM DESIGN

A beam-scanning system for the MPT was designed for verification. Figure 3 presents a block diagram of the beam scanning system with the algorithm in the previous section. Tx is a 4×4 DBF system composed of 16 channels operating at 5.8 GHz. The PC controls the operation of the entire DBF system. Based on the proposed algorithm, a baseband signal for beam scanning is generated using a digital signal processor. Following that, the generated baseband signal is converted to an analog signal using a digital-to-analog converter. The baseband signal is then frequency up-converted to a passband signal, amplified with high power, and radiated through an antenna.

A block diagram of the designed Rx is depicted in Fig. 4. It receives RF power via a 5.8-GHz channel, and the power is converted to DC power using an RF-DC converter. The transmitting CMM (T-CMM) is mounted on the Rx, and the rectified DC voltage value is applied to its analog-to-digital converter (ADC) and sampled. The single pole single throw (SPST) switch is located between the RF-DC converter and the PMIC to prevent the impedance change caused by circuit operation from affecting the voltage during scanning. In the pilot slots, the T-CMM opens the SPST and the voltages are sampled stably. Following the sampling of all scanning slots, the SPST is closed to store the received energy in the supercapacitor of the PMIC. To minimize power consumption, the

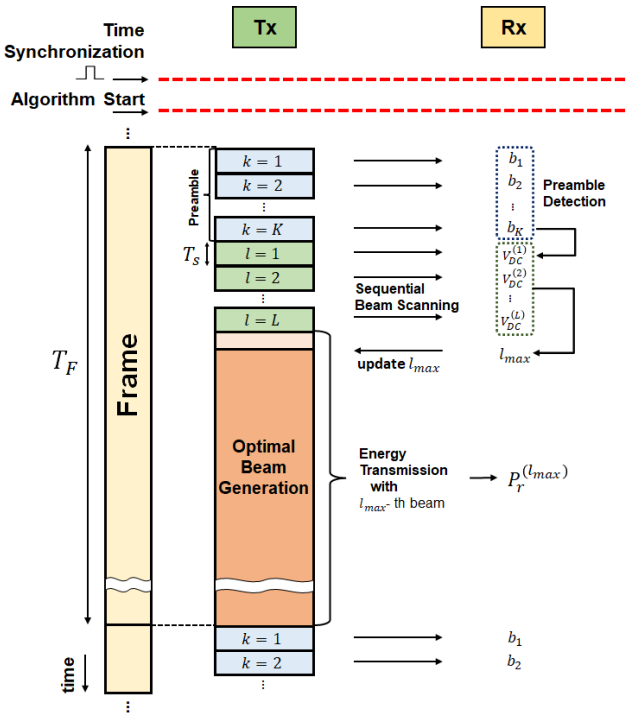

FIGURE 5. Operation timeline of Tx and Rx.

T-CMM enters sleep mode in an energy transmission slot and in idle time after sampling at each pilot slot.

Figure 5 shows the interaction between Tx and Rx in each frame. In the algorithm, the scanning beam radiated from the DBF system and sampled DC voltage should be time-synchronized by aligning the order. Therefore, a DBF system that performs beam scanning and the T-CMM require time synchronization. Prior to system operation, a pulse signal is connected to the DBF system and T-CMM. The DBF system and T-CMM recognize the rising edge of the pulse

and reset their respective internal timers. The two timers are gradually shifted owing to clock drift, and a preamble is included in front of the pilot slots to maintain the time synchronization. The preamble comprises K bits, and the Tx sends CW in a slot with bit '1' and does not send if the bit is '0'. By detecting the preamble from the trend of the sampled voltages, the T-CMM acquires information about the index for the start of beam scanning. Among the L sampled voltage values that follow, the index of the maximum voltage is selected as $l_{\max}$ and transmitted to the receiving CMM (R-CMM) in the Tx for receiving the index information. Based on the maximum index received from the T-CMM, the DBF system transmits energy by generating an optimal beam in the energy transmission slot.

B. FRAME STRUCTURE SETUP WITH SIMULATION

The proposed algorithm was simulated based on the system to be implemented in Section IV. The directivity of the antenna via simulation was 9.3 dBi and the spacing between

the antennas was 0.71 λ on the x-axis and 0.79 λ on the y-axis. It was assumed that the antennas in the DBF system radiated a signal of 30 dBm. The efficiency of the beam scanning algorithm was analyzed from $P = Q = 2$ to 15 for the number of pilot slots in a space, where $X = Y = Z = 1$ m. To obtain the received power, it was assumed that the position of Rx is at an arbitrary position in a plane separated from Tx by Z. Subsequently, the average received power can be expressed using the central limit theory (CLT), as follows:

$$X_i = P_{\max}^{(i)}, \tag{22}$$

$$P_{avg} = \lim_{N_{\mathrm{CLT}}\to\infty} \frac{X_1 + X_2 + \cdots + X_{N_{\mathrm{CLT}}}}{N_{\mathrm{CLT}}} = \lim_{N_{\mathrm{CLT}}\to\infty} \frac{1}{N_{\mathrm{CLT}}} \sum_{i=1}^{N_{\mathrm{CLT}}} X_i, \tag{23}$$

where $P_{\max}^{(i)}$ denotes the i-th sample for the received power according to the position of Rx, and N_{CLT} indicates the total number of samples. In a population with the sample, as in (22), based on the CLT, the average received power can be obtained as in (23).

It was confirmed that the average received power increased with the number of pilots. Based on the number of pilot slots $(K + L)$ and the time related to the frame structure $(T_{\mathrm{F}}, T_{\mathrm{s}})$, frame efficiency can be expressed as follows:

$$\eta_{\mathrm{frame}} = \frac{T_{\mathrm{F}} - (K + L)T_{\mathrm{s}}}{T_{\mathrm{F}}}. \tag{24}$$

Therefore, the average received power considering frame efficiency (η_{frame}) is expressed as follows:

$$P_{\mathrm{MPT}} = \eta_{\mathrm{frame}} P_{\mathrm{avg}}. \tag{25}$$

Figure 6 illustrates the simulation results of the average received power considering the frame efficiency with a T_{F} of 1 s and T_{s} of 1 ms. As depicted in Fig. 6, as the number of pilot slots increased, the time of the energy slot decreased, and consequently, the average received power decreased. It was confirmed that the optimal beam-scanning algorithm was possible when the number of pilot slots was 121.

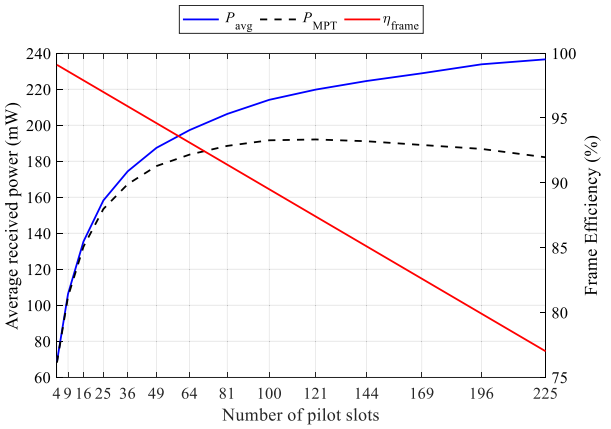

FIGURE 6. Average received power and frame efficiency according to the number of pilot slots.

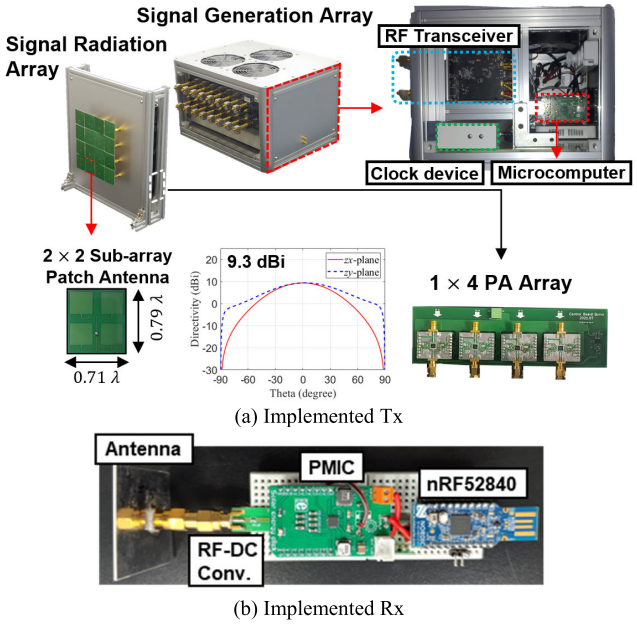

(a) Implemented Tx

(b) Implemented Rx

FIGURE 7. Implemented MPT system.

IV. EXPERIMENTAL VERIFICATION

A. SYSTEM IMPLEMENTATION

Figure 7 displays the implemented MPT system. More specifically, the DBF system includes a signal generation array (SGA) for generating an RF signal and a signal radiation array (SRA) for amplifying and radiating the signal. The DBF system was controlled using LabVIEW on the main PC connected externally and by microcomputers in the SGA. The main PC determined the operating state of the system and the microcomputers provide commands for the generation of signals to the SGA based on the state. Moreover, the SGA includes RF transceivers with a digital baseband processor and RF front-end and a clock distribution device (CDD) for the time and frequency synchronization of the RF transceivers. For the RF transceiver, USRP B210 with two

TABLE 1. Components used in the beam scanning system.

Name	Part number	Features
RF Transceiver	USRP B210	Channel: Tx 2, Rx 2 FPGA: Spartan 6 RFIC transceiver: AD9361
Micro-computer	Raspberry Pi 4B	USB 3.0 interface Raspbian OS
CDD	CDA-2990 (OctoClock)	8-ports 10 MHz, PPS
Power Amplifier	QPA9501	Qorvo Type: Class-AB Gain: 32 dB P1dB: 33 dBm
CMM	nRF52840 USB	Bluetooth version: 5.0
PMIC	BQ25570	MPPT, Boost charger, Buck converter
SPST	PI5A3167CCEX	On-Resistance: 0.8 Ω

channels of the transmit port, Raspberry Pi 4B for the micro-computer and CDA-2990 (Octoclock) for the CDD were used. A 1 × 4 array PA consisting of four layers was used to amplify the RF signal generated from the SGA. Qorvo's QPA9501 was employed for the array PA. The planar array antenna for radiating the RF signal was mounted on a 4 × 4 array.

The Rx has a channel for receiving an RF signal and includes an RF-DC converter circuit. This circuit was designed to rectify a 5.8-GHz signal with a power conversion efficiency of 68% at an input power of 18 dBm [16]. The PMIC stores energy from the RF-DC converter circuit in a supercapacitor, which is used to power the load and T-CMM. Moreover, an nRF52840 Dongle was utilized as the T-CMM to transfer the maximum index. It supports Bluetooth version 5 and communicates at 2.4 GHz. The receiving CMM (R-CMM) for receiving the maximum index was installed on the main PC of the DBF system. For the initial time synchronization, a 0.1-Hz pulse generated from the CDD was connected to the T-CMM for 10 s. Following the initial time synchronization, the time synchronization of the Tx and Rx continues in a wireless environment. The parts and features of the system are listed in Table 1.

B. EXPERIMENTAL SETUP

Two experiments were conducted to verify the implemented MPT system: beam scanning experiment and tracking experiment.

1) BEAM SCANNING EXPERIMENT

Figure 8 displays a photograph of the setup for the beam scanning experiment. In this experiment, the RSSI for each

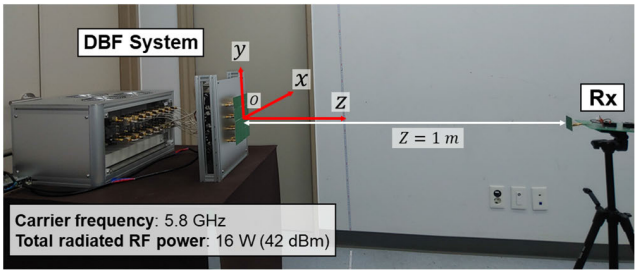

FIGURE 8. Beam scanning experiment Setup.

scanning beam is measured when the Rx is placed in a specific placement relative to the Tx. The radiated RF power from each channel was 1 W, and the total radiated power was 16 W (42 dBm). Moreover, the X, Y, and Z values were 1 m to set the direction of the beam in each index. For the preamble, $K = 5$ and $M_{\text{pre}} = N_{\text{pre}} = 2$ were set. Open circuit voltage values were measured according to the placement of Rx and L. A debugging probe was connected to the T-CMM to monitor the values in each index. The three placements for the Rx were as follows: (350 mm, 380 mm, 1000 mm) for Placement 1; (0, 0, 1000 mm) for Placement 2; and (-250 mm, -250 mm, 1000 mm) for Placement 3. For each placement, the orientation of the Rx antenna was directed toward the transmitter. For beam scanning, T_{s} was set as 10 ms, and the number of pilot slots in three cases was $P = Q = 4, 10, 15$ ($L = 16, 100, 225$).

2) TRACKING EXPERIMENT

A tracking experiment was conducted to verify that energy transmission can be performed by properly tracking the Rx moving in real time at every T_{F}. The setting values of preamble, transmission power, X, Y, and Z were the same as in the beam scanning experiment. For the frame structure, $L = 121$, $T_{\text{F}} = 1$ s, and $T_{\text{s}} = 1$ ms were applied. A rotation system based on a stepper motor was used to control the position of the Rx as illustrated in Fig. 9. On the rotation system, Rx rotates at trajectory of a radius of 400 mm on zx-plane. For the experiment, the center of rotation was placed at (0, 0, 600 mm) and the angular position θ_{Rx} changed according to the movement scenario. The RF power coupled from the directional coupler inserted between the RF antenna and RF-DC converter was measured every 40 ms using the power sensor. For comparison, measurements were performed on the case where the proposed algorithm was applied and the case where the beam direction was fixed at (0°, 0°).

C. EXPERIMENTAL RESULTS

1) BEAM SCANNING EXPERIMENT

The measurement results according to the placement of the Rx when $L = 100$ are depicted with simulation results in Fig. 10. The simulated value is the received RF power co-simulated by AWR Design Environment 16 and MATLAB R2020b based on (18). It can be confirmed that the rectified voltage and the received power are positively correlated, and

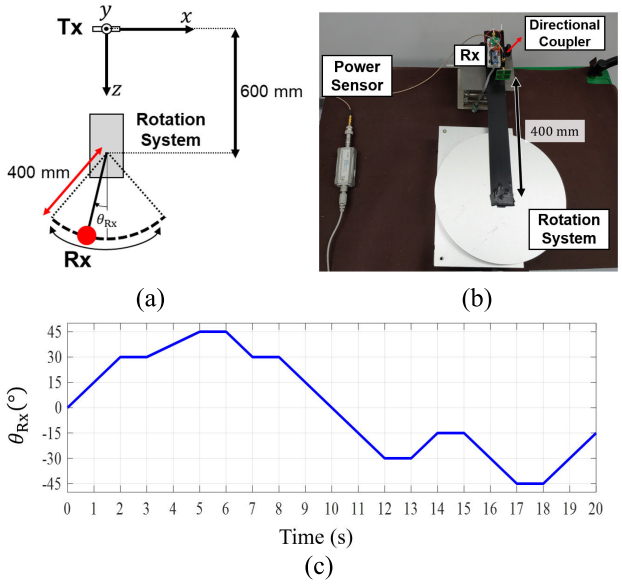

FIGURE 9. Tracking experiment setup: (a) Dimensions of the experimental setup (b) Measurement system photograph (c) Movement scenario.

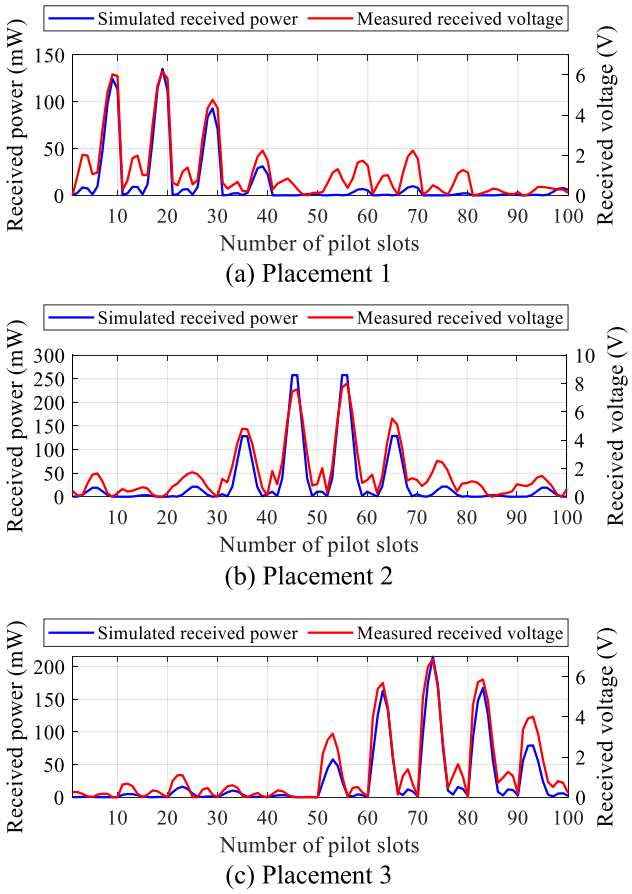

FIGURE 10. Measured received voltage and simulated power of L = 100.

the beam with the highest received power can be selected in all three placements. Moreover, the measured DC voltages for Placement 1 and Placement 2 are represented as the

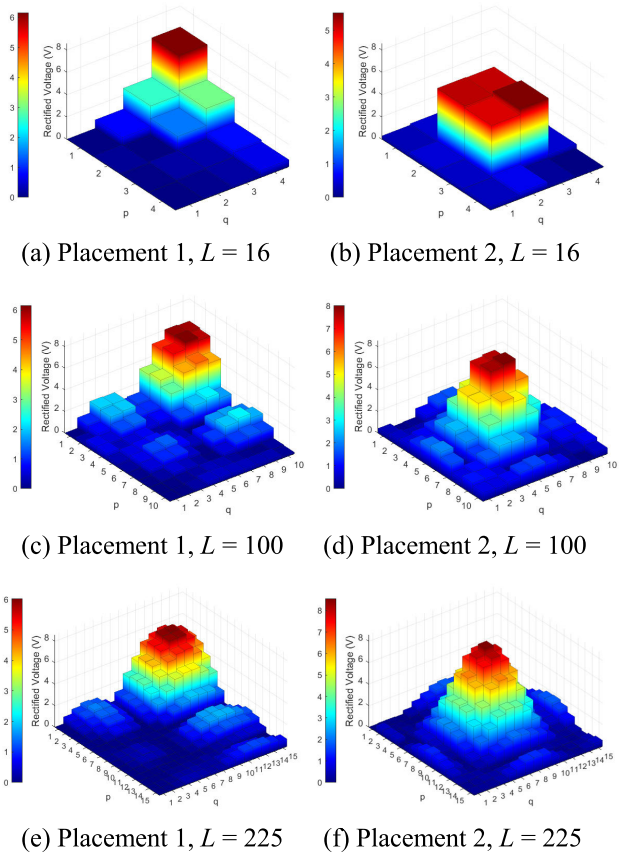

FIGURE 11. Colormaps of measured received voltage.

TABLE 2. Measurement results of beam scanning experiments.

	Maximum index			Maximum voltage (V)		
L	16	100	225	16	100	225
Placement 1	4	19	28	6.16	6.16	6.03
Placement 2	11	56	113	5.53	8.01	8.56
Placement 3	13	73	169	5.48	6.88	6.83

colormaps on the pq-plane in Fig. 11. It shows the rectified voltage distribution for the scanning beams according to L. Table 2 summarizes the maximum index and voltage based on the measured results. In Placement 1, even if L was 16, it was confirmed that the received voltage was similar to the case of $L = 100$ and $L = 225$ because the scanning beam for (1, 4) point is accurately performed at the location of the Rx. However, with the larger L, the direction of the beam can be selected with high resolution, which exhibits a tendency for the measurement results to be high.

2) TRACKING EXPERIMENT

Figure 12 presents the received RF power of the Rx obtained by considering the coupling of the coupler and insertion loss

TABLE 3. Comparison with other works.

Ref	Freq. (GHz)	Tx array	Beamforming scheme	Beamforming system	Feedback implementation	Tracking speed
[7]	5.2	4 × 8	LUT-based adaptive focal beamforming	Analog	Wired Feedback	N/A
[8]	5.8	8 × 8	Beam scanning	Analog	Wired Feedback	N/A
[9]	2.45	3 × 3	Auto-tracking CW time reversal	Analog	Wireless	0.8 s for tracking
[10]	0.915	1 × 2	Estimation from RSSI	Digital	Wireless	0.5 s per RSSI sampling
[11]	0.915	2 × 2	Blind-adaptive beamforming	Digital	Wireless	N/A
[12]	0.920	1 × 6	Kalman filter-based channel estimation	Digital	Wireless	several seconds for convergence
This work	5.8	4 × 4	Beam scanning with pilot slot analysis	Digital	Wireless	0.126 s for scanning

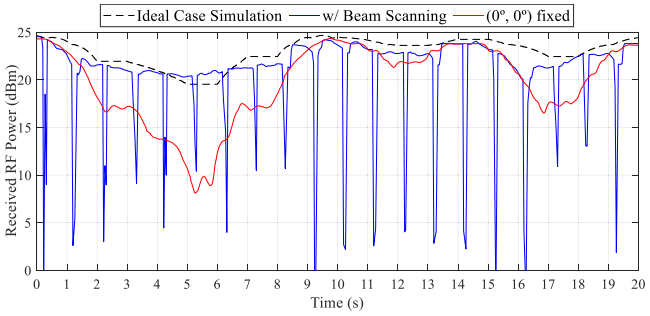

FIGURE 12. Rx Tracking experiment result.

of the line. This includes the simulation result, which is an ideal case for performing MPT on a consistently optimal beam based on (18). When the beam direction is fixed at (0°, 0°), the received power decreases as the receiver rotates to a higher absolute value of θ_{Rx}. The proposed algorithm receives higher power than the fixed case by performing beam scanning and then updating the beam direction. From 5 s to 6 s, θ_{Rx} was maintained at 40° for 1 s, and the average received power differed by 10.5 dB for the two cases. The validity of the proposed system was verified by comparing the measured result with the simulated result. Upon updating the beam direction every second, the experimental results of the implemented system closely match the simulation results of the ideal case.

D. COMPARISON WITH OTHER WORKS

Table 3 summarizes the results of the comparison with other studies. In [7] and [8], focal scanning methods were proposed and implemented to improve power transfer efficiency in the near field. However, these studies did not analyze the parameters of pilots suitable for beam scanning. In addition, verification in a complete wireless environment has not been conducted for actual operation. The authors of [9] proposed an algorithm to perform Rx tracking from a pilot signal when the received power falls below a certain level. Although the efficiency is high for a target with low mobility, because it takes 0.8 s to start tracking again, it has a low proportion of time available for the energy transmission of a continuously moving target. In [10], an algorithm that performs optimal beamforming by estimating each channel through RSSI was presented. The measurement and feedback interval per RSSI was set to 0.5 s considering the power consumption of Rx. In [11], blind-adaptive beamforming was proposed, which iteratively optimizes beamforming weight vectors using DBF system. Although it did not specify the time for Rx tracking, it presents aspects that can increase speed in the operation of the algorithm. The authors of [12] proposed an algorithm to perform optimal MPT for each placement of the Rx via Kalman filter-based channel estimation. As a result of moving the receiver at 1-min intervals, the convergence time was several seconds.

The MPT system proposed in this paper was verified in a completely wireless environment via time synchronization of the Tx and Rx. To maintain synchronization for a short time slot, the frame structure is operated based on baseband signal samples using DBF. The system selects the optimal beam from among the scanning beams at the frame period (1 s) and performs MPT.

V. CONCLUSION

In this study, a DBF system with real-time tracking for MPT is proposed. Based on the baseband signal generated by each channel, the time slots were configured in the frame structure to scan by rapidly switching the direction of the beam. Additionally, Rx rectified each scanning beam via the RF-DC converter, sampled the rectified voltage, and transmitted the index of the beam with the highest value to Tx. The Tx

then transmitted a beam corresponding to the received index to per-form MPT in the optimal direction. The Tx and Rx were time-synchronized in the wireless environment owing to the reset of both timers during the initial operation and a preamble included in the frame structure. The optimal number of scanning beams was derived by considering the average received power and proportion of the energy transmission slot in a frame.

For verification, a 4 × 4 DBF system operating at 5.8 GHz and Rx were designed. It was confirmed that the results of beam scanning in a fully wireless environment are consistent with the simulation. In addition, it was verified that the MPT can be performed in real time by tracking moving Rx every second. The proposed system can be effectively used to wirelessly supply power to mobile devices in an indoor environment.

REFERENCES

[1] C. T. Rodenbeck, P. I. Jaffe, B. H. Strassner, P. E. Hausgen, J. O. McSpadden, H. Kazemi, N. Shinohara, B. B. Tierney, C. B. DePuma, and A. P. Self, "Microwave and millimeter wave power beaming," *IEEE J. Microw.*, vol. 1, no. 1, pp. 229–259, Jan. 2021.

[2] A. Massa, G. Oliveri, F. Viani, and P. Rocca, "Array designs for long distance wireless power transmission: State-of-the-art and innovative solutions," *Proc. IEEE*, vol. 101, no. 6, p. 1464 1481, Jun. 2013.

[3] N. Shinohara, "History and innovation of wireless power transfer via microwaves," *IEEE J. Microw.*, vol. 1, no. 1, pp. 218–228, Jan. 2021.

[4] M. Wagih, A. S. Weddell, and S. Beeby, "Millimeter-wave power harvesting: A review," *IEEE Open J. Antennas Propag.*, vol. 1, pp. 560–578, 2020.

[5] K. Choi, D. Kim, and M. Y. Chung, "Received power-based channel estimation for energy beamforming in multiple-antenna RF energy transfer system," *IEEE Trans. Signal Process.*, vol. 65, no. 6, pp. 1461–1476, Mar. 2017.

[6] K. W. Choi, L. Ginting, A. A. Aziz, D. Setiawan, J. H. Park, S. I. Hwang, D. S. Kang, M. Y. Chung, and D. I. Kim, "Toward realization of long-range wireless-powered sensor networks," *IEEE Wireless Commun.*, vol. 26, no. 4, pp. 184–192, Aug. 2019.

[7] J. Bae, S.-H. Yi, H. Koo, S. Oh, H. Oh, W. Choi, J. Shin, C. M. Song, K. C. Hwang, K.-Y. Lee, and Y. Yang, "LUT-based focal beamforming system using 2-D adaptive sequential searching algorithm for microwave power transfer," *IEEE Access*, vol. 8, pp. 196024–196033, 2020.

[8] J. H. Park, N. M. Tran, S. I. Hwang, D. I. Kim, and K. W. Choi, "Design and implementation of 5.8 GHz RF wireless power transfer system," *IEEE Access*, vol. 9, pp. 168520–168534, 2021.

[9] L. Hu, X. Ma, G. Yang, Q. Zhang, D. Zhao, W. Cao, and B.-Z. Wang, "Auto-tracking time reversal wireless power transfer system with a low-profile planar RF-channel cascaded transmitter," *IEEE Trans. Ind. Electron.*, vol. 70, no. 4, pp. 4245–4255, Apr. 2023.

[10] S. Abeywickrama, T. Samarasinghe, C. K. Ho, and C. Yuen, "Wireless energy beamforming using received signal strength indicator feedback," *IEEE Trans. Signal Process.*, vol. 66, no. 1, pp. 224–235, Jan. 2018.

[11] P. S. Yedavalli, T. Riihonen, X. Wang, and J. M. Rabaey, "Far-field RF wireless power transfer with blind adaptive beamforming for Internet of Things devices," *IEEE Access*, vol. 5, pp. 1743–1752, 2017.

[12] K. W. Choi, L. Ginting, P. A. Rosyady, A. A. Aziz, and D. I. Kim, "Wireless-powered sensor networks: How to realize," *IEEE Trans. Wireless Commun.*, vol. 16, no. 1, pp. 221–234, Jan. 2017.

[13] X. Zhou, R. Zhang, and C. K. Ho, "Wireless information and power transfer: Architecture design and rate-energy tradeoff," *IEEE Trans. Commun.*, vol. 61, no. 11, pp. 4754–4767, Nov. 2013.

[14] C. A. Balanis, *Antenna Theory: Analysis and Design*. Hoboken, NJ, USA: Wiley, 2005.

[15] C. M. Song, S. Trinh-Van, S. H. Yi, J. Bae, Y. Yang, and K. Y. Lee, "Analysis of received power in RF wireless power transfer system with array antennas," *IEEE Access*, vol. 9, pp. 76315–76324, 2021.

[16] J. Kim, I. Park, and H. Ku, "Design of a highly efficient N-stage harmonic terminated voltage multiplier for wireless power transfer," *Energies*, vol. 14, no. 21, pp. 7203–7215, Nov. 2021.

MINJAE AHN (Student Member, IEEE) received the B.S. degree in electrical and electronics engineering from Konkuk University, Seoul, South Korea, in 2022, where he is currently pursuing the M.S. degree in electronics, information, and communication engineering. His research interests include wireless power transfer systems and RF front-end design.

INHO PARK (Member, IEEE) received the B.S. and M.S. degrees in electronic engineering from Konkuk University, Seoul, South Korea, in 2021 and 2022, respectively. He is currently a Researcher with Hanwha Systems. His research interest includes digital beamforming systems.

ILLSOO SOHN (Member, IEEE) received the B.S., M.S., and Ph.D. degrees in the field of electrical engineering from Seoul National University, Seoul, South Korea, in 2003, 2005, and 2009, respectively. He was a Postdoctoral Researcher with the Wireless Networking and Communication Group, The University of Texas at Austin, from 2009 to 2010. He was a Senior Research Engineer with the Advanced Communication Technology Research Laboratory, LG Electronics, from 2010 to 2012. He was a Network Design Engineer with the Network Strategy Department, KT Corporation, from 2012 to 2013. From 2013 to 2017, he was an Assistant Professor with the Department of Electronics Engineering, Gachon University. He is currently an Associate Professor with the Department of Computer Science and Engineering, Seoul National University of Science and Technology. His current research interests include statistical inference, message-passing algorithms, multi-user MIMO, multi-cell MIMO, time-division duplex, distributed antenna systems, and cross-layer optimization.

OH-SOON SHIN (Member, IEEE) received the B.S., M.S., and Ph.D. degrees in electrical engineering and computer science from Seoul National University, Seoul, South Korea, in 1998, 2000, and 2004, respectively. From 2004 to 2005, he was a Postdoctoral Fellow with the Division of Engineering and Applied Sciences, Harvard University, Cambridge, MA, USA. From 2006 to 2007, he was a Senior Engineer with Samsung Electronics, Suwon, South Korea. In 2007, he joined the School of Electronic Engineering, Soongsil University, Seoul, where he is currently a Professor. His research interests include communication theory, wireless communication systems, and signal processing for communication.

HYUNCHUL KU (Member, IEEE) received the B.S. and M.S. degrees in electrical engineering from Seoul National University, Seoul, South Korea, in 1995 and 1997, respectively, and the Ph.D. degree in electrical and computer engineering from the Georgia Institute of Technology, Atlanta, GA, USA, in 2003. From 1997 to 1999, he was with the Wireless Communication Research Center, KT Corporation, Seoul. From 2004 to 2005, he was with the Research and Development Laboratory, Mobile Communication Division, Samsung Electronics, Suwon, South Korea. Since 2005, he has been a Professor with Konkuk University. His research interests include digital RF systems, RF power amplifiers, RF front-end design, and wireless power-transfer systems.